Design and Evaluation of a Low-Speed Wind-Tunnel with Expanding Corners

by

Björn Lindgren & Arne V. Johansson

Department of Mechanics

October 2002
Technical Reports from
Royal Institute of Technology
Department of Mechanics
SE-100 44 Stockholm, Sweden

Typsatt i $\mathcal{AMS}$-LaTeX med Osos *rapport*-stil.

Universitetsservice US AB, Stockholm 2002

Contents

Design and evaluation of a low-speed wind-tunnel with expanding corners

By Björn Lindgren and Arne V. Johansson

Dept. of Mechanics, KTH, SE-100 44 Stockholm, Sweden

Technical report. TRITA-MEK 2002:14

A new low-speed closed circuit wind-tunnel has been designed and built at the Royal Institute of Technology, Stockholm. It has a test section with a cross section area of 0.5×0.75 m^2 and a length of 4.2 m. The maximum speed is about 48 m/s with empty test section. The contraction ratio is 9. A heat exchanger, a honeycomb and 5 screens are included to minimize flow disturbances in the test section. The streamwise turbulence intensity in the test section is less than 0.04% in the core with similar values for the cross stream turbulence intensities. The variation in total pressure is less than $\pm 0.1\%$ and the variation in temperature is less than $\pm 0.07^\circ$C over the cross section area and $\pm 0.03^\circ$C in time in the centre of the test section. The concept of expanding corners, with a substantially larger outlet than inlet cross section area, ($e = 1.316$), has been implemented successfully with a total pressure-loss coefficient in the first corner downstream the test section of 0.047 at a guide-vane chord Reynolds number of 205000. This value is a two-dimensional estimate obtained from measurements in a centre plane downstream the vanes. It compares favorably with the total pressure-loss coefficient in most wind-tunnels using non-expanding corners. Together with the good flow quality found in the test section this proves the usefulness of expanding corners in modern wind-tunnels to minimize the overall size for a given test section length.

1. Introduction

Wind-tunnels represent a useful tool for investigating various flow phenomena. An advantage of using wind-tunnels is that experiments there can be performed under well controlled flow circumstances compared to experiments in the open environment. The drawback is that small scale models often have to be used instead full scale ditto. To achieve the same Reynolds number as for the real application, the kinematic viscosity or flow velocity normally has to be changed. In most wind-tunnels air at atmospheric pressure is used, and the only option left is to increase the flow velocity. Often it is not possible to increase the velocity enough, so the results from wind-tunnel experiments fall in between

those achievable in most well resolved simulations and the real application on a Reynolds number scale. There are however some large wind-tunnels used in the auto and aircraft industries. These tunnels have test sections that can accomodate full scale vehicles and small aircraft.

There are many types of wind-tunnels and they can be classified by *e.g.* flow speed dividing them into four groups.

- subsonic or low-speed wind-tunnels
- transonic wind-tunnels
- supersonic wind-tunnels
- hypersonic wind-tunnels

Subsonic or low-speed wind-tunnels are the most common type and the wind-tunnel described in this paper is of this type. Transonic wind-tunnels are common in the aircraft industry since most commercial aircraft operate in this regime. Supersonic wind-tunnels can be used to investigate the behavior of jet engines and military aircraft. Hypersonic wind-tunnels find their applications in rockets and space vehicles. A further way to categorize low-speed tunnels is by dividing them into open circuit or closed circuit wind-tunnels. In open circuit wind-tunnels there is no use for corners and long diffusers but the power needed to drive the wind-tunnel is high because of the loss of energy in the out-flowing air. Closed circuit wind-tunnels recirculate the air and thus normally need less power to achieve a given flow speed, see section 2, and, above all, facilitate the achievement of well controlled flow conditions in the test section. The present, and most low-speed tunnels used for research, are of the closed circuit type.

Wind-tunnel design is a complex field involving many fluid mechanics and engineering aspects and it is impossible to cover them all in just one paper. Some books and articles have been written about this topic and *e.g.* Rae & Pope (1984), Bradshaw & Pankhurst (1964) are useful references when designing and constructing low-speed wind-tunnels. See also the comprehensive report on the German-Dutch Wind-tunnel edited by Seidel (1982).

The first wind-tunnel at the Royal Institute of Technology was completed in the summer of 1932 at a newly constructed laboratory for aeronautical sciences. It had a closed circuit and an open jet test section, *i.e.* the test section had no walls. The test section was cylindrical in shape with a diameter of about 1.6 m and a similar length. It was primarily used for measuring forces on aircraft models and airfoils. It had an axial fan and corners with simple guide-vanes made of bent plates in the shape of $\frac{1}{4}$-circles. The contraction ratio was about 5 and the maximum speed in the test section about 50 m/s, see Malmer (1933). It was later modified with, among other things *e.g.* a closed test section, and was in use until only a few years ago.

A number of other wind-tunnels for aeronautical research have existed over the years at KTH. Another low-speed tunnel, (formerly known as L2 now

L2000), was built in 1963 and is still used for aeronautical research. It has a 3 m long test section of 2×2 m^2 cross section and a maximum speed of 62 m/s. A supersonic, a hypersonic and a ballistic wind-tunnel are also part of the early aeronautical research history at KTH. In 1990 the MTL low-turbulence low-speed tunnel was inaugurated.

The present tunnel complements the MTL-tunnel in several respects, both in research projects and in teaching. In particular it fulfills the need of a test section with very flexible design to allow *e.g.* strong pressure gradients etc.

The limited available space made it necessary to use innovative design ideas that could allow a large enough test section for research projects, such as high Reynolds number turbulent boundary layer studies, into a small size wind-tunnel. There are some possibilities to reduce the overall size of a closed circuit wind-tunnel without making the test section smaller. One obvious way is to decrease the contraction ratio, CR, *i.e.* the ratio between the largest cross section are, (found in the stagnation chamber), and smallest cross section area, (found in the test section). Most large wind-tunnels already have quite small contraction ratios though, $CR \leq 6$. One should keep in mind that a high contraction ratio is a key factor in achieving a good flow quality. Another way to reduce size is to use wide-angle diffusers. The use of wide-angle diffusers is a fairly common method to reduce the overall circuit length. The resulting losses, though, are rather high and accompanied by increased level of flow disturbances. Finally there is also the possibility to use expanding corners which is used in this wind-tunnel.

Expanding corners have a larger outlet than inlet cross section area reducing the need for long diffusers, see section 2.3, and can thus reduce the total wind-tunnel circuit length by about 20% without a large increase in total pressure-loss. The idea of using expanding corners has been around for a long time, *e.g.* Friedman & Westphal (1952), Collar (1936), Wolf (1957) and Kröber (1932) made some interesting experiments on expanding bends. However, most of the early results were not too encouraging, so the idea was put aside until recently. One of the reasons for the unfavorable results were the use of simple guide-vane shapes. When there is a large expansion, (expansion ratio of *e.g.* 1.316), in such a short distance a lot of effort has to go into the design of the guide-vanes to avoid boundary layer separation and a large total pressure-loss. Today, some new or planned wind-tunnels use expanding corners both at universities and in the automobile industry. The concept of expanding corners is especially useful in large wind-tunnels, because of the reduction in the total wind-tunnel circuit length.

The design of the guide-vanes used in the present wind-tunnel has primarily been made using the MISES code developed by Harold Youngren and Mark Drela at MIT, see *e.g.* Drela & Youngren (1995). This code solves the coupled

Euler- boundary layer equations on an infinite array of guide-vanes to compute the two-dimensional flow field. This method allows for small boundary layer separation bubbles but cannot handle large separations. The code was developed for turbo machinery applications and some compressibility has to be introduced for convergence. The main advantage using the MISES code is that it has a built-in optimization tool which allows the user to specify the pressure field on the guide-vane surface and from that obtain the desired the guide-vane shape to fit the specified pressure profile. This facilitates the optimization substantially. For more information on the code and its mathematical methods see *e.g.* Drela & Youngren (1995), Youngren & Drela (1991), Giles & Drela (1987), Drela & Giles (1987).

The use of expanding corners also has implications on other parts in the wind-tunnel circuit. The diffusers in this wind-tunnel are two-dimensional, or plane, *i.e.* the expansion is only in one plane. This type of diffusers are more sensitive to boundary layer separation than their three-dimensional counterparts leading to a smaller maximum opening angle and thus a longer diffuser for a given area increase. This removes a small part of the gains made in wind-tunnel circuit length by using expanding corners. There has been numerous investigations on two-dimensional diffusers and their optimum shape, *e.g.* Fox & Kline (1962), Reneau *et al.* (1976), Çabuk & Modi (1992), Ganesan *et al.* (1991). The diffusers here have straight walls for simple manufacturing.

2. The wind-tunnel design

In 1995 it was decided to build a new low-speed wind-tunnel as a complement to the larger MTL wind-tunnel already operating at the Department of Mechanics, KTH, Stockholm, see Johansson (1992) and Lindgren & Johansson (2002).Aside from reducing the user load on the larger MTL wind-tunnel by the purpose of the new tunnel was also to give the undergraduate students the possibility to work with a new state of the art wind-tunnel. A primary aim was to here accommodate experiments that require a large degree of flexibility of the test section geometry. To meet these requirements it was necessary to specify design criteria that are close to those of the MTL wind-tunnel thereby simplifying the transfer of projects between the two wind-tunnels. The main design criteria are listed in the table below,

① Closed circuit wind-tunnel.
② Good flow quality (mean flow variation, turbulence intensities & temperature variation).
③ Contraction ratio, CR, of 9.
④ Test section aspect ratio of 1.5 and the maximum test section length possible in the available space.
⑤ Maximum flow speed in the test section of at least 40 m/s.
⑥ Low noise level.
⑦ Low cost.

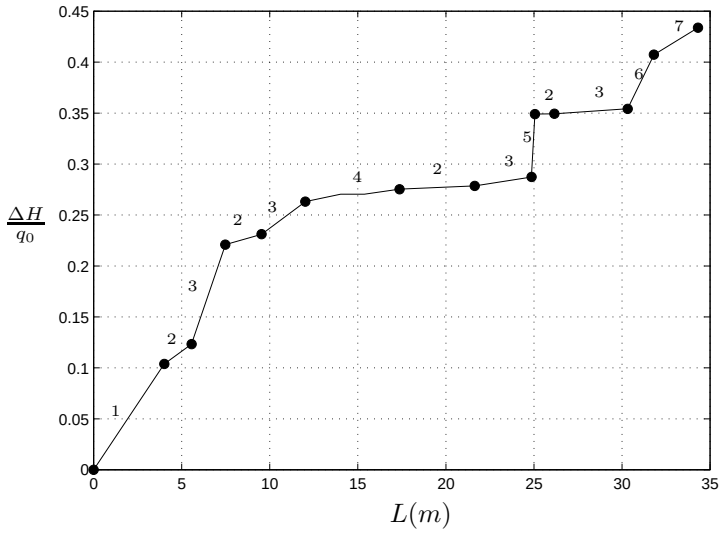

FIGURE 1. An estimate of the cumulative total pressure-loss coefficient for each part in the wind-tunnel at a test section speed of 40 m/s. See table 2 and figure 2 for numbering of wind-tunnel parts.

① A closed circuit wind-tunnel gives better control of the flow conditions such as temperature and pressure and it also reduces the necessary power to run the wind-tunnel at a given speed compared to an open wind-tunnel. In addition it improves the environment with lower noise levels and avoids air blowing around the laboratory.
② To achieve good flow quality it was decided that the stagnation chamber should have one honeycomb and five screens. It was also decided that the wind-tunnel should be equipped with a heat exchanger. This is the same configuration as in the MTL wind-tunnel, see Johansson (1992).
③ To improve the flow quality and to make use of the well-proven contraction shape of the MTL wind-tunnel it was decided that the contraction ratio, which is the ratio between the largest, (stagnation chamber), and the smallest, (test section), cross section area in the wind-tunnel circuit, should be equal to 9.
④ The test section aspect ratio was chosen to be identical to that in the larger MTL wind-tunnel to simplify the transfer of projects between the two wind-tunnels. The maximum possible cross section area in the test section with $CR = 9$ is 0.5×0.75 m^2 because of space limitations. The length of the test section was chosen to be around 4 m to be able to get a high enough Reynolds number on a flat plate. This size of test section was made possible by the use of expanding corners, see section 2.3 and Lindgren *et al.* (1998)

⑤ Most of the experiments planned for this wind-tunnel are aimed for speeds of about 25 m/s in the test section. To allow for increasing flow resistance due to measurement equipment such as flat plates, cylinders and traversing equipment the design goal for the maximum speed was set to 40 m/s.
⑥ A large fan running at low rpm and silencers around the fan were expected to be sufficient to achieve low noise levels in the tunnel and the surrounding laboratory.
⑦ All the design and construction of the wind-tunnel parts were made in-house, using the previously acquired knowledge from the construction of the MTL wind-tunnel keeping the total cost of the wind-tunnel to a minimum.

A computer program was written to calculate the size of the individual wind-tunnel parts, the pressure variation and pressure-loss variation around the wind-tunnel circuit. These calculations were made to decide the appropriate motor for the fan and the necessary cooling power to keep the temperature steady at full speed with a set temperature of about room temperature. The calculated total pressure loss coefficient around the wind-tunnel circuit is shown in figure 1. It can be seen that the parts contributing most to the overall loss are the test section, the first expanding corner downstream of the test section, (denoted as corner 1 in this paper), the heat exchanger and the stagnation chamber with the screens and the honeycomb. This illustrates the dilemma where increasing flow quality also means increasing total pressure-loss. Therefore when comparing the total pressure-loss coefficient for different wind-tunnels it is important to bear in mind the length of the test section and what flow quality improving devices are included, *e.g.* air cooler and number of screens.

By measuring the dynamic pressure in the test section, q_1, for a variation of fan rpm the power factor, λ, of the wind-tunnel can be estimated. The power factor is a measure of the total pressure-loss of the wind-tunnel circuit and can be compared to the computed total pressure-loss shown in figure 1. It is defined as follows,

$$\lambda = \frac{\Delta p_{tot}}{\eta_f q_1} = \frac{P_m \eta_m}{A_1 U_1 q_1} \tag{1}$$

where Δp_{tot} is the total pressure-loss of the wind-tunnel circuit, P_m is the power input from the motor, A_1 is the test section cross section area, U_1 is the test section flow speed and η_f, η_m are the fan and motor efficiency factors respectively. In table 1 the test section velocity, the power input and the power factor are presented for different fan rpm values. It can be seen that for low rpm the power factor is very high, indicating large losses in the wind-tunnel circuit, and for high rpm the power factor approaches a constant value, which in this case is about 0.45. It should be compared to the estimated value of the power factor of 0.44 at 40 m/s. One can also compare it with the value of the power factor for the MTL wind-tunnel which is about 0.39 at 69 m/s, see Johansson &

TABLE 1. The power input, P_m, the test section speed, U, and the power factor, λ, for fan rpm values from 100 to 1000.

rpm	100	200	300	400	500	600	700	800	900	1000
P_m kW	0.02	0.12	0.38	0.83	1.57	2.67	4.19	6.19	8.79	12.0
U m/s	3.5	8.1	12.7	17.4	22.2	27.1	32.0	36.9	41.8	46.6
λ	1.97	0.89	0.72	0.61	0.56	0.53	0.50	0.48	0.47	0.46

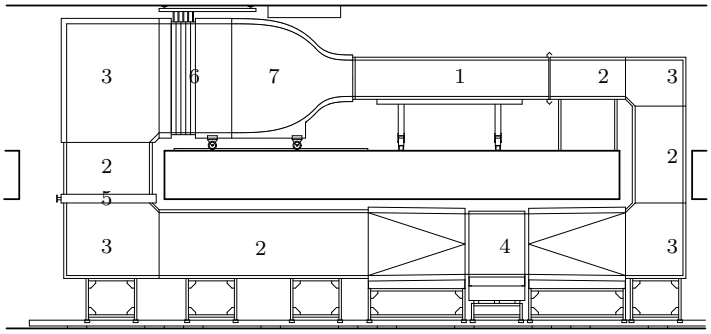

FIGURE 2. The wind-tunnel layout. For description of the numbered parts see table 2.

Alfredsson (1988). The comparison with the MTL wind-tunnel and the trend showing decreasing power factor with increasing test section speed, illustrate the two major influences on the power factor, namely the importance of the size of the wind-tunnel and at what test section speed the value of λ is calculated. A number of design features, especially the number of screens, the length of the test section and the presence of a heat exchanger also have a large influence on the value of λ, (see figure 1). Hence one should keep these effects in mind when comparing the power factor of different closed circuit wind-tunnels.

In the following sections a short description of the wind-tunnel parts is presented. They can be seen in figure 2.

2.1. *Test section*

The highest velocity in the tunnel circuit occurs in the test section resulting in a large contribution to the total pressure-loss from skin friction on the walls. Also disturbances from models, plates etc in the test section will substantially contribute to the pressure-losses. It is therefore important to remember this when choosing the length of the test section and when the test section accessories, such as traversing system etc are designed. Another effect of disturbances in

TABLE 2. A description of the wind-tunnel parts. See also figure 2. (A = cross-section area, L = length, e = expansion ratio, D = diameter, P = power, CR = contraction ratio.)

Part	Description
1.	Test section, $\left(A = 0.5 \times 0.75 \text{ m}^2,\ L = 4.2 \text{ m}\right)$
2.	Two-dimensional diffuser
3.	Expanding corner, $\left(e = \sqrt[8]{CR} \approx 1.316\right)$
4.	Fan, $(D = 1.25 \text{ m},\ P = 15 \text{ kW})$
5.	Cooler, $(P = 17 \text{ kW})$
6.	Honeycomb, screens & stagnation chamber
7.	Contraction, $(CR = 9)$

the test section is that it can lead to flow separation in the diffuser directly downstream of the test section, (referred to as diffuser 1 in this paper), and in corner 1. This is a reason for a somewhat conservative design of the first diffuser. The size of the test section is 0.5×0.75 m^2 in cross section area and 4.2 m in length. This is the maximum possible length due to space restrictions. For a given cross section the length of the test section should not be made too large in order to avoid too much influence on the core flow from the wall boundary layers.

To be able to set the pressure gradient along the centerline of the test section one wall is adjustable to vary the cross section area in the downstream direction. Previous experience from the operation of the MTL wind-tunnel and the difficulty there to adjust the pressure gradient made us choose one adjustable wall instead of two as in MTL. With two opposite adjustable walls a movement of one wall affects the flow at the other wall leading to a time consuming iterative process before the desired pressure gradient is achieved with sufficient accuracy. The entire side of the test section containing the adjustable wall can be replaced making the test section more flexible and facilitating experiments that require major changes of the test section, see *e.g* Angele (2000). Two walls are also equipped with hatches to improve access to the interior of the test section. The test section is made of a steel frame for stiffness with plywood top and bottom, and the side walls, including the adjustable wall, made of Plexiglas®.

2.2. *Diffusers*

In this wind-tunnel the diffusers are plane or two-dimensional. This is a result of using expanding corners where all the expansion in one plane around

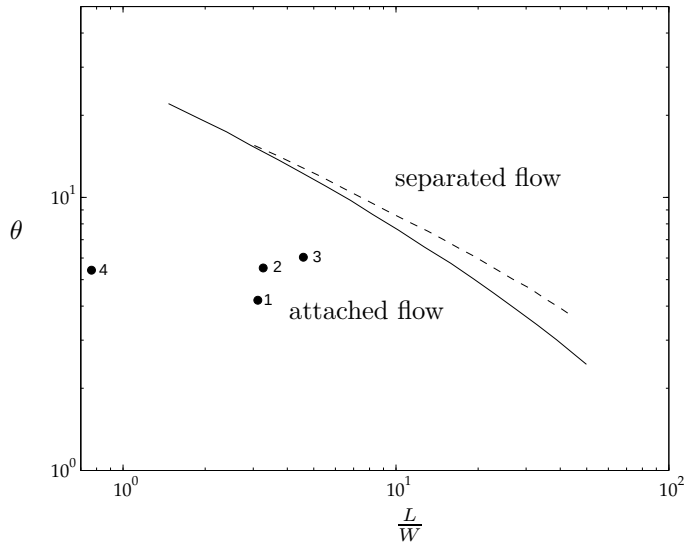

FIGURE 3. Separation of two-dimensional diffusers. −−: Line of maximum pressure recovery, —: Line of separation, •: The diffusers in this wind-tunnel numbered from the test section following the flow. L=length, W=width and θ=total opening angle. The lines are taken from Fox & Kline (1962).

the wind-tunnel circuit is accommodated in the corners, see section 2.3. Two-dimensional diffusers are less efficient in recovering static pressure and less resistant to boundary layer separation than three-dimensional diffusers. Therefore two dimensional diffusers have to have a smaller opening angle leading to a longer diffuser for a given expansion. Consequently, the reduction of the wind-tunnel circuit length achieved by the use of expanding corners is partly lost by the fact that it is accompanied by two-dimensional diffusers.

The thickness of the inlet boundary layers and non-uniformities of the inlet velocity profiles are also important factors, see Waitman *et al.* (1961) and Wolf (1969), when setting the diffuser opening angle. Thick diffuser wall boundary layers separate easier than thin boundary layers. In figure 3, the line of separation, (solid line), is plotted as a function of the ratio between diffuser length and width, (according to Fox & Kline (1962)). In that case, however, the boundary layer thickness at the diffuser inlet is small and in this wind-tunnel circuit they are usually quite thick. As an example the thickness of the inlet boundary layers in the diffuser following corner 1 is about 10 cm. Therefore it is important not to design diffusers with opening angles too close to the separation line. The diffusers in this wind-tunnel are represented in the figure as filled circles and they are numbered in the downstream direction. Diffuser number

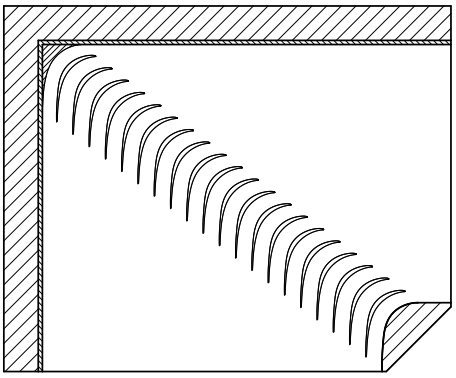

FIGURE 4. First corner in the flow direction from the test section. The flow is from right to bottom. $e = A_{\text{out}}/A_{\text{in}}$

4, located downstream the heat exchanger, see figure 2, is not as close to the line of separation as desired but other geometrical restrictions also influenced the design of the diffusers. The optimum wall shape of a diffuser has a larger opening angle at its entrance and a decreasing opening angle thereafter. Here, however, all diffusers have straight walls to simplify the manufacturing.

The dashed line in the figure is the line of maximum pressure recovery, (according to Fox & Kline (1962)). The reason for this line to be located into the regime with separation that is the friction-loss on the diffuser walls decreases and the increase in pressure-loss due to a small separation is relatively small. For optimization of plane diffusers the reader may also wish to consult Reneau *et al.* (1976), Çabuk & Modi (1992) and Ganesan *et al.* (1991).

An extra benefit with plane diffusers is that they can easily have adjustable diffuser walls so that the expansion in the diffuser can be changed. This is especially useful in the diffuser following the test section. The test section has an adjustable wall so that the user can set the pressure gradient in the streamwise direction, see section 2.1. It is then useful to adjust the diffuser wall as well, which is possible in plane diffusers that have two parallel walls, to fit the cross section area to that of the test section. Hereby, it is possible to make measurements on *e.g.* a flat plate closer to the exit of the test section and in this way increase the maximum Reynolds number on *e.g.* a flat plate.

2.3. *Corner*

The idea of using expanding corners has been around for a long time, see *e.g.* Collar (1936) and Kröber (1932), but it was always discarded since the early experimental results were not too encouraging. One of the reasons for the

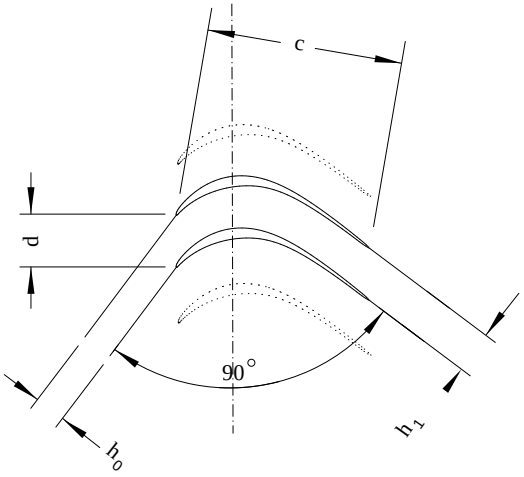

FIGURE 5. The geometry of a cascade of 90° turning guide-vanes. c = vane chord, d = spacing between vanes, h_0 = inlet distance between vanes, h_1 = outlet distance between vanes & $e = h_1/h_0$ = is the expansion ratio.

discouraging results is the simple guide-vane shapes that were used then. The most common shape used in wind-tunnels for a long time has been the $\frac{1}{4}$-circle with a constant thickness and with a straight prolongation at the trailing edge (sometimes also at the leading edge). In more recent investigations guide-vanes with varying thickness were used, although the shapes of the suction and pressure sides were still simple and often of circular shape, see *e.g.* Friedman & Westphal (1952) and Wolf (1957).

The major benefit of using expanding corners is the larger size of the test section that can be fitted into a wind-tunnel for a given circuit length without an increase in total pressure-loss for the wind-tunnel circuit. Other benefits are reduced friction loss, the possibility to use diffusers with variable diffuser angle and the possibility to have a larger fan radius leading to lower fan rpm and thus lower blade tip speed and consequently less noise. The reason for the larger fan and the reduced friction loss is the rapid expansion achieved by the first two corners which are located fairly close to the test section in the downstream direction. With a compact design of the circuit we have a short first diffuser exposing corner 1 to the disturbed flow from the test section which emphasizes the importance of well designed guide-vanes optimized for the expansion ratio used.

In this case the guide-vane used in the MTL wind-tunnel developed by Sahlin & Johansson (1991) was used as a starting shape for the development of a new guide-vane optimized for the expansion ratio used in this wind-tunnel and a chord Reynolds number of 200000, see Lindgren *et al.* (1998). The procedure of developing the new guide-vane was to look at the pressure profile on the original vane. Its performance here was, as expected, not totally satisfying with *e.g.* laminar separation bubbles on each side of the guide-vane profile. In an iterative process, where the guide vane profile was altered gradually, a pressure profile was achieved which was free from separation bubbles and without transition to a turbulent boundary layer on the pressure side.

These calculations were made using the MISES cascade code and its inverse optimization tool, see Drela & Youngren (1995) and Lindgren *et al.* (1998). Inverse optimization means that a new pressure profile that is not too different from the pressure profile found in the previous iteration is specified and the guide-vane shape matching the new pressure profile is then calculated. Step by step a larger change in pressure profile and guide-vane shape are achieved.

The new guide-vane was then tested at varying Reynolds numbers and inlet flow conditions. These tests lead to some minor changes of the guide-vane shape such as increased nose radius and reduced camber. It also slightly increased the calculated cascade pressure-loss coefficient, which is a measure of the total pressure-loss in the corner, from 0.039 to 0.041. The value determined from experiments was found to be slightly higher, see section 4.5.

Figure 4 shows a cut through corner 1. The expansion ratio in all corners in this wind-tunnel is $\sqrt[8]{9} \approx 1.316$ where 9 is the contraction ratio, CR, of the wind-tunnel. Hence, the 4 corners account for a total expansion of $\left(\sqrt[8]{9}\right)^4 = 3$, leaving only a factor of 3 in expansion to be handled by the diffusers. Note that the shape of the corner inner and outer walls mimic the suction and pressure shapes of the guide-vane. This is important because the flow then sees the cascade as infinite. However, there is also a negative effect on the performance of the guide-vanes from the corner wall boundary layers. The rapid expansion in the corners lead to a very rapid increase in boundary layer thickness, see section 4.5. The influence of the wall boundary layers is neglected when the total pressure-loss coefficient of the guide-vane cascade is measured for comparison with the calculations.

The guide-vanes are separated by a distance, d, of 0.3 times their chord length, c, see figure 5. This is not the optimum spacing for maximum static pressure recovery, see Lindgren *et al.* (1998), but it guarantees a satisfactory capability of avoiding boundary layer separation on the vanes if the inlet flow condition is poor. This is especially important in this wind-tunnel because of the short diffuser between the test section, where large disturbances can be generated by measurement equipment, and corner 1.

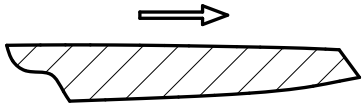

FIGURE 6. The shape of the guide-vane trailing edge. The flow tends to curl up from the lower side of the guide-vane with higher pressure towards the upper suction side which means that there should be a sharper angle at the corner closest to the lower side. The arrow indicates the flow direction.

The guide-vanes are made of extruded aluminum and they are mounted to the inside of the corner walls. Two expanding pins run through a laser cut plate into the short end of the guide-vane. A center screw then fixes the guide-vane to the plate. This way of fixing the guide-vanes in the corners ensures that their position and angle of attack is very accurate.

In the first three corners the guide-vane angle of attack is fixed, but in the fourth corner there is a possibility to adjust it by a few degrees to compensate for deviations in flow direction. The adjustment is made individually for each guide-vane. There are both pros and cons with this arrangement. There is an obvious advantage of being able to adjust the flow direction for compensating possible local flow misalignment. On the other hand it is difficult and time consuming to make these changes and once the wind-tunnel is calibrated the guide-vane angle of attack will probably never be altered.

To avoid an oscillating flow separation point at the trailing edge of the guide-vane causing high levels of noise at a distinct frequency, the trailing edge of the guide-vane should be cut as shown in figure 6. The noise is generated by the von Kármán vortex street behind a blunt trailing edge. There are also other mechanisms that can generate noise. One suggestion is that there is an interaction between Tollmien-Schlichting generated boundary layer instabilities that are strongly amplified on the pressure side close to the trailing edge. These instabilities then roll up to form a von Kármán type vortex street with the same frequency as the noise, see Nash *et al.* (1999). It is important that the trailing edge corner close to the pressure side of the guide-vane is sharper than the corner on the suction side since the flow wants to curl around the trailing edge from the pressure to the suction side.

2.4. *Machinery*

The control of the test section speed, *i.e.* fan rpm, and temperature is fully automated by the use of computers, current controlled valves and a fan control unit. A computer located near the test section is used to enter the desired values

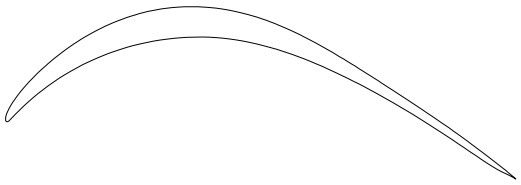

FIGURE 7. The new guide-vane developed for an expansion ratio of 1.316. Observe that the trailing edge is not modified from calculations.

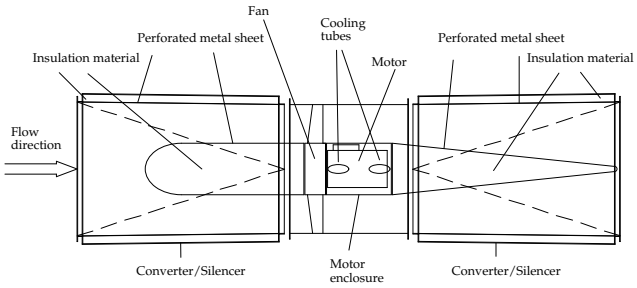

FIGURE 8. The fan located in between the two silencers.

for velocity and temperature. This can either be done manually, by using the keyboard, or from another computer through an ethernet connection. The entered set values are then sent to a NI Field Point control system by serial RS 232 communication. This Field Point system consists of four modules. One for data communication and power supply, one for digital output signals, one for analog output signals and one for temperature input signals, (PT-100). The digital output is used to start and stop the fan and the cooling circuit pump and the analog output is used for automatic control of fan rpm and cooling system valves.

2.4.1. *Driving unit*

The fan configuration is shown in figure 8 . It is located downstream the second corner, see figure 2. The fan is positioned between a pair of silencers. They also transform the cross section shape of the wind-tunnel circuit between circular, (the parts nearest to the fan), and rectangular. Some expansion is also taking

place in the silencers to keep the total wind-tunnel circuit length to a minimum. In the center of the silencers, cylinder shaped bodies made of perforated steel plate and filled with acoustic insulation material are mounted. In the upstream silencer the cylinder has a constant diameter and its nose is shaped as half an ellipsoid, see figure 8. The central body in the downstream silencer is shaped as a cone, see figure 8, to avoid flow separation. The central bodies improve the flow quality both upstream and downstream of the fan. They also improve the noise reduction capability of the silencers. The insulation material is (long-fibered) glasswool® and it is separated from the air flow by a perforated steel plate. The sound waves can thus penetrate into the insulation material, through the holes in the steel plates, where they are absorbed. The thickness of the insulation layer is 10 cm.

The motor delivers 15 kW of power. It is mounted axially behind the fan and it is enclosed in a steel plate cylinder to minimize the disturbance on the flow. Therefore, extra air for cooling the motor is provided from outside the wind-tunnel circuit through two cylindrical pipes.

The fan diameter is 1.25 m and the hub diameter is 0.5 m. The fan has 8 blades with an angle of attack of 53°. With this angle of attack and an empty test section the fan efficiency is close to its maximum value of 75%. The blades do not enter the stall region even at considerably higher loads, making sure that the wind-tunnel efficiency and flow quality stays intact during the operation of the most common kinds of experiments. The adjustment of the blade angle of attack was done during the wind-tunnel calibration, see section 4.1.

The use of axial fans can, however, create some flow quality problems, if they are subjected to very high loads, but even with more moderate loads they can create a low frequency pulsating variation of the streamwise flow component. In the present tunnel this is essentially, but not completely, avoided by a relatively low fan blade load.

2.4.2. *Cooling circuit*

One of the primary measurement techniques used in this kind of wind-tunnel is the **C**onstant **T**emperature **A**nemometry, CTA. Since the idea of this measurement technique is to keep the hot-wire at constant temperature, a change in the surrounding air flow temperature will affect the cooling of the wire and, will thus be interpreted as a change in velocity. Therefore it is very important to have a stable, well determined temperature in the test section. This is achieved by including a heat exchanger, *i.e.* an air cooler, into the wind-tunnel circuit. This heat exchanger consists of elliptical pipes with cooling flanges through which cold water is flowing at a constant rate. The air blows perpendicularly through the grid of cooling pipes.

The main problem with using a heat exchanger of this type is that it is one of the parts that contributes most to the total pressure-loss of the wind-tunnel

circuit, see figure 1. Therefore it is important to install it where the cross section area of the wind-tunnel circuit is as large as possible. This would indicate an optimum position in the stagnation chamber, see figure 2. On the other hand it is important to give the flow time to even out spatial temperature variations and therefore the heat exchanger should be installed far away from the test section. The compromise between these goals resulted in the positioning of the heat exchanger between corner 3 and diffuser 4, see figure 2. Here the cross section area is sufficiently large to keep the pressure-loss at an acceptable level and it is far enough from the test section so that the spatial temperature variation has time to even out. There is also the option of using turbulence generators on the cooling pipes to improve the heat transfer but they increase the pressure-loss radically and the turbulence they generate deteriorates the flow quality significantly. This option was therefore rejected.

A schematic view of the cooling circuit is shown in figure 9 and the parts are described in table 3. As seen in figure 9 the system is divided into three parts. The first part is the wind-tunnel circuit with its flow of air. The air is cooled by water flowing through a heat exchanger in the second part. This part consists of a closed loop of piping where the water flows at a constant rate. The way of changing the heat flux from the air to the water is therefore by changing the water temperature. The reason for doing it this way, instead of changing the water flux, is that a high flow rate through the heat exchanger results in a better air temperature uniformity over the cross section. The final part is the external cooling water system of the building. It consists of a high pressure and a low pressure side with a water temperature of about 10°C on the high pressure side. This water cools the water in the closed loop, (second part), through another heat exchanger. The flow rate from the high to the low pressure side is controlled by a current-controlled valve. By keeping the closed loop circuit length to a minimum and using a high flow rate the response time of the whole system can be minimized resulting in small temporal air temperature variations in the test section and shorter transient times at changes in the set temperature and set velocity. Finally there is a shunt pipe bypassing the heat exchanger, see figure 9, in the closed loop circuit to be used in more advanced control techniques than the PID regulator system now in use.

2.5. *Stagnation chamber & contraction*

2.5.1. *Stagnation chamber*

The stagnation chamber, located downstream corner 4, is the part of the wind-tunnel circuit that has the largest cross section area. This part has a major influence on the flow quality in the test section. Because of the high local pressure drop generated by flow improving devices it is important to position them in the location with the lowest flow speed and thereby minimize their contribution to the total pressure drop of the wind-tunnel circuit. In the present

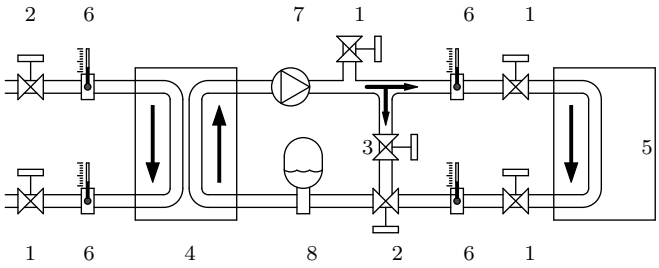

FIGURE 9. The water cooling circuit in the wind-tunnel. The outer, (left in figure) part is an in-house cold water system and the inner, (right in figure) part is a closed circuit loop with the flow controlled by the user. For numbering of parts see table 3.

TABLE 3. A description of the cooling circuit parts. See also figure 9

Part	Description
1.	Stop valve
2.	Current controlled regulator valve
3.	Throttle valve in shunt pipe
4.	Water to water heat exchanger
5.	Water to air heat exchanger
6.	Thermometer, (PT-100)
7.	Pump with maximum pressure rise of 35 m H_2O (0.35 MPa)
8.	Expansion tank

wind-tunnel the stagnation chamber is equipped with one honeycomb and five screens.

The honeycomb used here is 75 mm long and the hexagonally shaped cells have a diameter of a quarter of an inch or 6.4 mm, *i.e.* the length to diameter ratio of the cells is about 12. The primary reason to use a honeycomb is that, with a sufficient length of about 10 cell diameters, see Bradshaw & Pankhurst (1964), it is a very effective flow straightening device. The relatively low pressure drop of a honeycomb makes it rather ineffective in reducing non-uniformities or fluctuations in the streamwise component but it is very effective in reducing cross-stream components, see *e.g.* Scheiman & Brooks (1981). This is especially useful in wind-tunnels with expanding corners since the low guide-vane chord Reynolds number in the last corner increases the risk

of boundary layer separation on the suction side of the guide-vanes. A honeycomb also breaks up eddies larger than the cell size and reduce the free-stream turbulence level, see *e.g.* Loehrke & Nagib (1976).

The use of screens to improve flow quality in wind-tunnels was first proposed by Prandtl (1932). The screens are very effective in breaking up larger eddies and acts primarily to reduce mean non-uniformities and fluctuations of the streamwise component. The screens also reduce cross-flow components but less effectively than honeycombs. Hence, the combination of honeycomb and screens provide, in a natural way, a good overall flow quality improvement.

By using a cascade of screens with subsequently finer mesh the turbulence and mean flow variation can be reduced substantially, see Groth (1991). In the wind-tunnel there are five screens with varying mesh size, see table 4, where M is the mesh size and d is the wire diameter, see also figure 10. Screens also reduce flow angle deviations. The relationship between the inflow angle, θ, and the out flow angle, ϕ, is,

$$\phi = \alpha\theta, \tag{2}$$

where α is a constant between 0 and 1. Empirically, see Laws & Livesey (1978), α is related to the local pressure-loss coefficient, K_0, through the following expression,

$$\alpha = \frac{1.1}{\sqrt{1+K_0}}. \tag{3}$$

The local pressure-loss coefficient, K_0, is determined by the solidity of the screen, $\sigma = 1 - \beta$, and the wire diameter Reynolds number, Re_{d},

$$K_0 = f\left(Re_{\mathrm{d}}\right)\frac{1-\beta^2}{\beta^2}, \tag{4}$$

derived by Laws & Livesey (1978). The function $f(Re_{\mathrm{d}})$ in equation 4 has a strong Reynolds number dependence for low Reynolds numbers, ($Re_d < 100$), but it is almost constant, with a value of about 0.5, for high Reynolds numbers, see Groth & Johansson (1988). The solidity, $1 - \beta$, is here between 0.3 and 0.4. At high Reynolds numbers, ($Re_d > 100$), the flow over the screen wires is supercritical. This means that small scale turbulence is generated by the wires in the screen. Although the reduction in flow variation is less for supercritical than sub-critical screens it is preferable not to use sub-critical screens because of their very large pressure drop. A series of supercritical screens with consecutively smaller mesh is more effective in reducing flow variations and turbulence than a single sub-critical screen, and with a smaller pressure drop, see Groth (1991). The distance between the screens needs to be larger than about 30 mesh sizes, for the wire generated turbulence to decay sufficiently, see Groth & Johansson (1988).

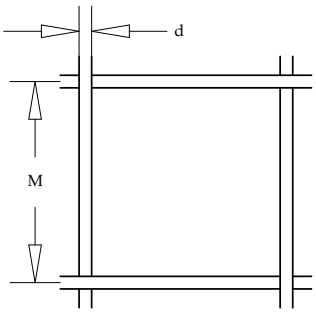

FIGURE 10. Definition of mesh width, M, and wire diameter, d.

The porosity, β, is defined as,

$$\beta = \left(1 - \frac{d}{M}\right)^2, \tag{5}$$

where M is the mesh size and d is the wire diameter, see figure 10. The values of M, d and β for the screens used in this wind-tunnel are presented in table 4.

The reduction in the streamwise mean flow variation can also be expressed in terms of α and K_0. The expression derived by Taylor & Batchelor (1949) reads

$$\frac{\Delta u_2}{\Delta u_1} = \frac{1 + \alpha - \alpha K_0}{1 + \alpha + K_0}, \tag{6}$$

where Δu_1 is the variation in streamwise velocity upstream the screen and Δu_2 is the variation in streamwise velocity downstream the screen.

The reader may notice that the expression in equation 6 equals zero for $K_0 = 1 + 1/\alpha$. It would be ideal to be able to eliminate the flow variation this way but equation 6 is only valid for solidities below 0.45 and the solidity required for equation 6 to be zero is 0.63. The reason for equation 6 to become invalid is a phenomenon called jet-collapse, see *e.g.* Baines & Petersen (1951). It occurs when the jets flowing out through the screen holes merge and form larger jets and structures. This leads to large variations in the flow and thus, must be avoided. The values of the porosity of the screens used in this wind-tunnel is presented in table 4.

When the flow has passed through the last screen it has been exposed to a substantial strain, which gives an anisotropic state with most of the turbulence energy in the cross-stream components. It is therefore important to allow it

TABLE 4. Data for the screens and the honeycomb used in the new tunnel at a test section flow speed of 40 m/s.

Screen	d $[mm]$	M $[mm]$	β	Re_d	K_0	f
1	0.71	3.2	0.61	210	0.80	0.50
2	0.56	2.4	0.58	165	0.99	0.55
3	0.56	2.4	0.58	165	0.99	0.55
4	0.16	0.7	0.61	47	1.71	0.75
5	0.16	0.7	0.61	47	1.71	0.75
honeycomb	0.075	6.35	0.97	29	-	-

to relax towards an isotropic state before entering the next part in the wind-tunnel circuit, which is the contraction. Just as the screens, the contraction is most effective in reducing streamwise fluctuations and in particular mean velocity variations.

The relaxation takes place in a straight part of the wind-tunnel circuit with constant cross section area (settling chamber), which is 0.75 m long in this wind-tunnel.

2.5.2. *Contraction*

The final, and for flow quality improvement, maybe most important, part in the wind-tunnel circuit is the contraction through which the flow passes before entering the test section. In the contraction the flow is accelerated rapidly. This results in a large streamwise strain, that reduces mean flow variations and the larger the contraction ratio, CR, the larger the strain and thus reduction. In this wind-tunnel the contraction ratio is 9.

The contraction can be divided into two parts. The first part has walls of concave shape and it is very important to elongate this part as much as possible to avoid wall boundary layer separation to occur here. The risk for separation is caused by the streamline curvature effects on the pressure gradient in the boundary layer. Along a fair part of this section there will be a positive pressure gradient see *e.g.* Seidel (1982). The generation of Görtler vortices decreases the risk for separation because the vortices inserts fluid with higher momentum into the boundary layers, see Görtler (1941) but they will not prevent separation completely if the contraction curvature is to sharp. The second part of the contraction has convex walls. Here, there is also a risk of separation close to the test section since there is a positive pressure gradient here as well, see *e.g.* Seidel (1982). It is easy to counteract a separation in this section by using some boundary layer tripping device such as tape with V-shaped roughness elements, (used in the MTL wind-tunnel). A separation in the first part is very difficult to eliminate though through tripping etc. The location of the contraction, just upstream of the test section, makes it very important to achieve a high quality

contraction design. The shape used in this wind-tunnel is taken from the MTL wind-tunnel and it was derived by Henrik Alfredsson and Alexander Sahlin at the department through inviscid/boundary layer calculations optimizing the pressure gradient along the contraction walls. It resulted in a shape described by:

$$f = A\left(\sinh\left(B\frac{x}{L}\right) - B\frac{x}{L}\right), \qquad \frac{x}{L} \leq 0.7 \tag{7}$$

$$f = 1.0 - C\left(\sinh\left(D\left(1-\frac{x}{L}\right)\right) - D\left(1-\frac{x}{L}\right)\right), \qquad \frac{x}{L} > 0.7 \tag{8}$$

where $A = 0.205819$, $B = 3.52918$, $C = 0.08819$ and $D = 8.23523$. x is the downstream coordinate and L is the contraction length. Here L is 2.5 m. The height and width are given by

$$H = \pm h\left(\sqrt{CR}\left(1 - f\left(\frac{x}{L}\right)\right) + \frac{1}{2}f\left(\frac{x}{L}\right)\right) \tag{9}$$

$$B = \pm b\left(\sqrt{CR}\left(1 - f\left(\frac{x}{L}\right)\right) + \frac{1}{2}f\left(\frac{x}{L}\right)\right) \tag{10}$$

where $h = 0.75$ m is the test section height and $b = 0.5$ m is the test section width. Further information on design and optimization of contractions can be found in *e.g.* Downie *et al.* (1984), Borger (1976) and Mikhail & Rainbird (1978).

The reduction of the variation in mean flow velocity in the contraction is very large

$$\frac{\Delta u_1}{U_1} = \frac{\Delta u_0}{CR^2 U_0}, \tag{11}$$

$$\frac{\Delta v_1}{U_1} = \frac{\Delta v_0}{\sqrt{CR}U_0}, \tag{12}$$

where U is the mean velocity in the streamwise direction and Δu and Δv are the velocity variations in the streamwise and crosswise directions, respectively. Subscripts 0 and 1 indicate positions at the upstream and downstream ends of the contraction respectively. As seen in equations 11 and 12 the reduction is much larger for the streamwise component, as it scales with the contraction ratio squared, than for the crosswise component that scales with the square root of the contraction ratio. For a contraction ratio of 9, as in this wind-tunnel, the reduction of the streamwise velocity component is 81 times the initial variation and for the crosswise components it is 3 times the initial variation. This simple inviscid theory can also be used to give a first rough estimate of the reduction of turbulence, (by replacing Δu with u_{rms} etc). The basis for a better, but still inviscid and linear, theory is the assumption that the strain-rates for the

turbulent fluctuations are much smaller than those for the mean flow components, see Batchelor (1976). The relations 11 and 12 can then be modified for this, so called, rapid distortion theory as follows

$$\frac{\Delta u_{rms1}}{U_1} = \frac{1}{CR^2}\sqrt{\frac{3}{4}\left(\ln\left(4CR^3\right)-1\right)}\frac{u_{rms0}}{U_0}, \tag{13}$$

$$\frac{\Delta v_{rms1}}{U_1} = \sqrt{\frac{4}{3CR}}\frac{v_{rms0}}{U_0}, \tag{14}$$

However, for geometries such as that of the present contraction effects of viscous dissipation are non-negligible. The formulas 13 and 14 would give reduction factors of 35.4 and 3.7, respectively, for u_{rms}/U and v_{rms}/U. From the study of Sjögren & Johansson (1998) we find that realistic values of these factors should be 36.4 and 9.1. In this case the rapid distortion theory works quite well for the streamwise component but the error is large in the cross stream component. This can mainly be contributed to a large dissipation in the beginning of the contraction. This dissipation is present in both components but has a larger influence on the cross stream component. At the end of the contraction there is also a redistribution of energy from the cross stream component to the streamwise component.

3. Experimental setup

The experiments concerning flow quality in the test section, *e.g.* mean flow, temperature and turbulence intensity measurements, were performed at a position 250 mm from the inlet of the test section. A special traversing arm was built, see figure 11, made of three joints connected by two beams. The beams are made of extruded aluminum with a laminar airfoil profile. Trip tape was applied to the beams to eliminate flow instability induced noise, see *e.g.* Nash *et al.* (1999). The axes were all orientated in the streamwise direction allowing movements in the cross stream plane of the traversing arm. One joint was mounted on the test section wall, one joined the two beams and one was located at the far end of the outer beam allowing rotation of a 500 mm long sting. This was a necessary feature to allow control of the rotational direction of the probe. The sting is long enough to keep the probe upstream of the flow field influenced by the traversing arm.

All three axes were equipped with DC servo controlled motors that could be operated from a computer, automating the traversing process. On the inner axis there was also a balance weight mounted to counteract the gravitational force on the traversing arm.

Two coaxial cables and two pressure tubes that can be connected to a probe run inside the beams and the sting, thereby minimizing flow disturbances.

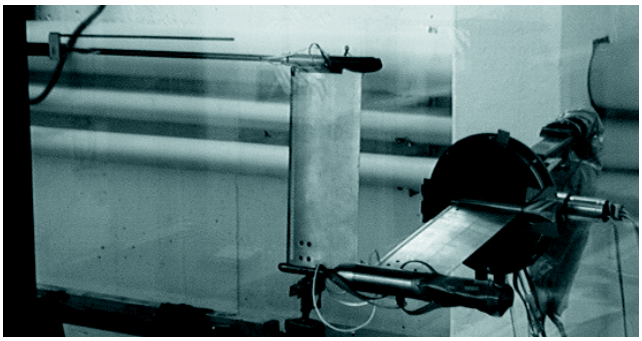

FIGURE 11. The traversing system used for measurements in the cross section of the test section at a position of 250 mm downstream the entrance of the test section.

Cables supplying power and encoder information for the motors also run inside the beams.

The probes used in the experiments at this location were single-wire and cross-wire probes for measuring the turbulence intensities and mean velocity components in the streamwise and the two cross-stream directions. A PT-100 probe for measuring the temperature fluctuations and a Prandtl tube for total pressure measurements were also used.

The single wire was calibrated in the free-stream over a large enough velocity range using King's law

$$U_0 = \left(\frac{E^2 - A}{B} \right)^{\frac{1}{n}} \tag{15}$$

where U_0 is the free-stream velocity, A, B and n are constants to be determined and E is the voltage output from the anemometer. The velocity was determined using a Prandtl tube measuring the dynamic pressure and by measuring static pressure and temperature of the air.

The cross-wire probe was calibrated in a similar way using a fifth order polynomial instead of King's law. In that case an extra device allowing variation of the probe angle was mounted onto the sting. The streamwise and cross stream velocities were determined by

$$U = U_0 \cos \alpha, \tag{16}$$

$$V = U_0 \sin \alpha, \tag{17}$$

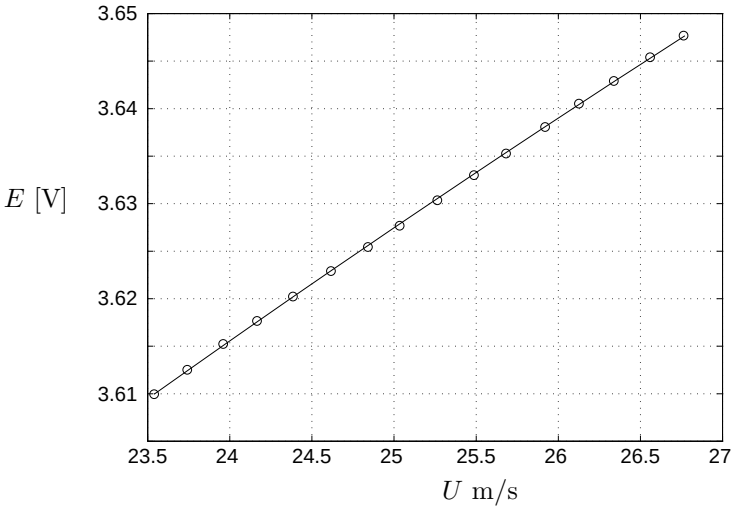

FIGURE 12. The calibration of a single-wire. The circles are measured points and the solid line is the King's law derived by a least square fit to the measured points.

where U and V are the streamwise and cross stream velocity components respectively and α is the probe angle. Two new variables, x and y were constructed from the wire voltages E_1 and E_2 as follows

$$x = E_1 + E_2, \tag{18}$$

$$y = E_1 - E_2, \tag{19}$$

The variables x and y were then used to construct two polynomials of fifth order, denoted M and N, for the two variables, U and $\tan\alpha$. By solving the equations

$$MA = U, \tag{20}$$

$$NB = \tan\alpha, \tag{21}$$

the coefficients in the vectors A and B can be determined. They are then used when the measurement data in form of voltages are converted to velocities.

Figures 12 and 13 show the results from one single wire and one cross-wire calibration. Note that all samples during a measurement have to be inside the end points of the calibration curve for the single-wire case and inside the area bounded by the solid lines for the cross-wire case.

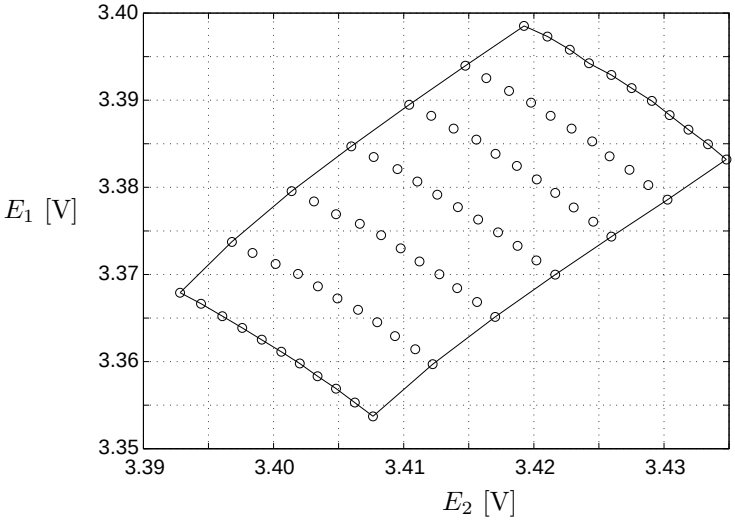

FIGURE 13. The calibration of a cross-wire. The circles are measured calibration points and the solid lines represent the area within which all measurement points must lie.

The error in U for the single-wire calibrations was less than $\pm 0.1\%$ and for the cross-wire calibration it was less than $\pm 0.1\%$ for the streamwise, U, component and the cross stream components V and W.

For the temperature measurements a PT-100 probe was mounted at the end of the sting. By using three of the four wires available for cross-wire measurements and connecting them to the NI Field Point temperature unit, described in section 2.4, with a built-in wire compensation the temperature could be measured across the cross section area. The temperature probe permanently mounted in the test section for controlling the wind-tunnel air temperature was used for the temporal variation measurements. The accuracy of the temperature sensors was about 0.4 °C in absolute value but the relative accuracy is much higher.

For the pressure measurements a differential pressure transducer from Furness Controls was used. It communicated with the computer via an RS-232 serial port. It has a built in averaging function for up to 20 sec of averaging and the relative accuracy at low pressure differences is less than 0.1 Pa.

Some measurements were performed downstream of corner 1 to verify the results in earlier experiments and calculations of guide-vane performance, see Lindgren *et al.* (1998). In this setup a different traversing system was used. It consists of a bar running horizontally through the diffuser downstream of

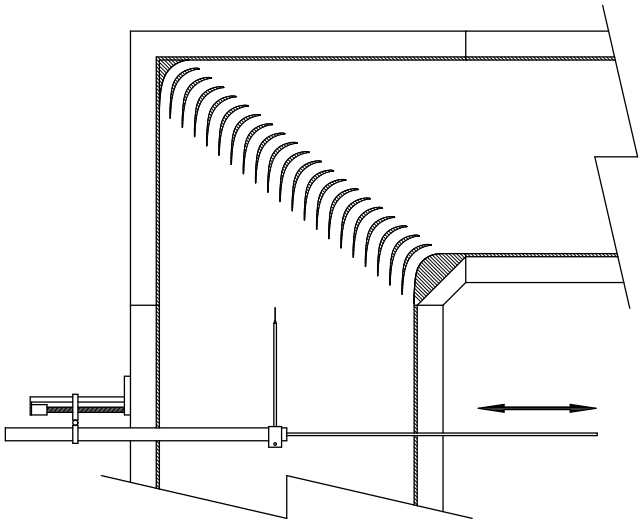

FIGURE 14. The traversing arm behind corner 1. The axis of motion is, as the arrow indicates, horizontal.

corner 1. The bar holds a sting with a pitot tube pointing vertically at its end, see figure 14. The pitot tube was positioned in the mid spanwise plan and it could be traversed across the array of guide-vanes using a servo controlled DC motor. This enabled quasi two-dimensional measurements of the guide-vane wakes behind the corner and calculation of the corresponding total pressure-loss of the corner. The static pressure upstream and downstream the corner also had to be measured. When measuring the static pressure at a wall it is very important that the pressure holes are not damaged in their edges. Therefore plugs were made containing the pressure holes and these were carefully flush-mounted in the wall to avoid disturbances, see Shaw (1960).

Finally noise measurements outside the test section and the fan were performed with a hand held dB meter. It was done during a time of the day when outer noise disturbances were at a minimum. Still there is a fair contribution from other noise sources, such as ventilation etc, to the results at low test section speeds.

4. Results

When investigating the results of the design and construction of a wind-tunnel there are several key factors that have to be checked carefully. The most important factors concern mean flow variations in time and space over the test section cross section area, the turbulence fluctuation intensities, both in the

streamwise and cross-stream directions, and temperature variations in time and over the same cross section area.

A mean flow variation in time would indicate problems with the fan or with static pressure changes. This kind of problems can be eliminated by changing *e.g.* fan blade angles or by increasing the flow through the pressure equalizing slit downstream the test section. Mean flow non-uniformities can originate from *e.g.* separation on some of the corner guide-vanes, diffuser separation or by flow blockage due to inefficient screens or honeycomb. If these deficiencies are small the problems can be taken care of by the contraction but larger deficiencies and problems generated in the contraction are difficult to eliminate, see section 2.5.2.

High turbulence levels often originate from small separations or deficient screen and honeycomb design, *e.g.* through jet collapse, see section 2.5.1.

Large temperature variations in time suggest an insufficient control system and large variations in space that the heat exchanger is located too close to the test section or that the water flow rate is not large enough.

All these factors were investigated and the results are presented in the following section.

Noise measurements were also performed outside the wind-tunnel. Static pressure variation measurements inside the test section are very difficult to perform without getting excessive influence from the dynamic pressure variations, see Johansson (1992). Static pressure fluctuations are present as sound waves traveling both in the upstream and downstream directions around the wind-tunnel circuit, see Michel & Froebel (1988). However, in low speed wind-tunnels the contribution to the streamwise velocity fluctuation from the static pressure fluctuations is small. Equation 22 shows an estimate of the contribution from static pressure variations.

$$\left(\frac{u_{\mathrm{rms}}}{U}\right)_{\mathrm{p_{rms}}} = \frac{C_{\mathrm{p_{rms}}} M}{2} \tag{22}$$

The mach number, M, is small and the pressure coefficient, $C_{\mathrm{p_{rms}}} = p_{\mathrm{rms}}/q$ is usually also small for low-speed wind-tunnels making the contribution small, (q is the dynamic pressure, p is static pressure and u is the streamwise velocity component). In the MTL wind-tunnel efforts were made to measure the static pressure fluctuation intensity and it was found to be below $0.00015q$, see Johansson (1992). With $C_{\mathrm{p_{rms}}} < 0.00015$ and $M = 0.072$ it results in a contribution of less than 5×10^{-4} % to the total velocity fluctuation.

The measurements in the test section in this article are confined to the core region of the test section. For the case of *e.g.* boundary layer experiments on a flat plate it will also be relevant to investigate the velocity variation in the streamwise direction along the test section length and the two-dimensionality of

the flat plate boundary layer, see *e.g.* Mehta & Hoffmann (1987) and Österlund & Johansson (1999).

Aside from measurements in the test section an investigation of the performance of the expanding corners was made. Here, the velocity in the test section was chosen so that the vane chord Reynolds number was about 200000 to enable comparisons with the calculations and experiments earlier performed by Lindgren *et al.* (1998).

4.1. *Total pressure measurement*

The total pressure variation in the test section is a measure of the uniformity of the flow. It is defined as

$$\frac{\Delta p_t(y,z)}{q_1} = \frac{p_{t1}(y,z) - p_{t0}}{q_1} \tag{23}$$

where $p_{t1}(y,z)$ is the total pressure in the test section, p_{t0} is the total pressure in the stagnation chamber at a fixed position and q_1 is the dynamic pressure in the test section at a fixed position, (*e.g.* the centerline). The reason for choosing the total pressure in the stagnation chamber as a reference pressure is that it is very stable in time.

The results at a free-stream velocity of about 25 m/s is shown in figure 15. The maximum variation was found to be less than $\pm 0.1\%$ which is satisfactorily low. It can be compared to the total pressure variation in the MTL wind-tunnel which also has a peak to peak variation of $\pm 0.1\%$, see Johansson (1992) and Lindgren & Johansson (2002). It is interesting to note that a total pressure variation of $\pm 0.1\%$ corresponds to a velocity variation of $\pm 0.05\%$. The location of the contours shown in figure 15 has a fair uncertainty because of the difficulty in measuring these extremely small pressure differences.

The small variation in the mean flow is here achieved by the use of screens and a contraction ratio as high as 9. As explained in section 2.5 a careful choice of mesh sizes and solidities for the screens and a contraction with high contraction ratio reduce the mean flow variation to a very low level. The results here and the design of these parts are similar to those in the MTL wind-tunnel for which the flow quality has been shown to be very good, see Johansson (1992) and Lindgren & Johansson (2002).

As part of the tuning of the wind-tunnel the angle of attack of the fan blades was adjusted to achieve a suitable loading on the blades, and to ensure that boundary layer separation does not occur on them. This is crucial in order to achieve a good flow uniformity. A separation pattern can vary in time and with blade, leading to a pulsating flow in the test section. The load on the fan blades is also determined by the total pressure-loss of the wind-tunnel circuit. An increasing pressure-loss increases the blade load. The adjustment of the blades and the corresponding variation in flow behavior is described in some

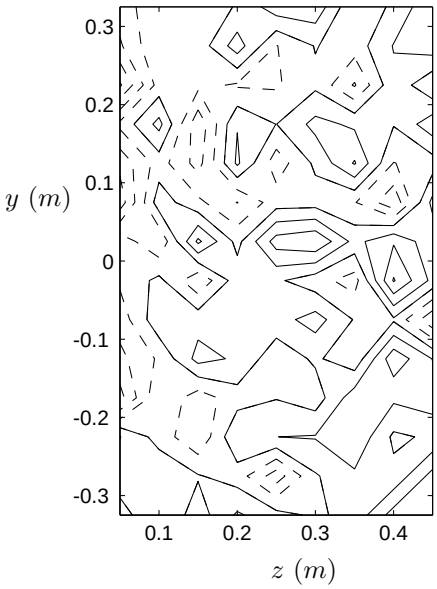

FIGURE 15. The total pressure variation in a cross section area of the test section located 0.25 m from its entrance. Each line represents an increment of 0.025%. Dashed lines are negative values and solid lines positive values.

detail in Lindgren (1999). With a blade angle of attack of 53° a separation free flow was achieved and the fan efficiency factor, η_f,was about 75%.

4.2. *Temperature measurement*

When using measurement techniques depending on heat transfer, such as hot-wire anemometry, it is very important that the temperature in the test section is well controlled and uniform over the entire cross section area, and stable in time. To investigate these variations in the new wind-tunnel a Pt-100 temperature probe was traversed over the cross section area at the same position as where the total pressure measurements were made, see section 3. The variation in time was measured at the test section centerline for a test section velocity of about 25 m/s and a set temperature of about 1°C below ambient temperature.

The temperature variation over the cross section area is presented in figure 16. The maximum variation is $\pm 0.07\ ^{\circ}C$. The location of the contours has a fair amount of uncertainty due to the difficulties in measuring the temperature with very high accuracy. The variation in time has a non-negligible effect on the spatial variation. However, there is a clear distinction between two areas with higher temperatures in the lower and left parts of figure 16 and lower

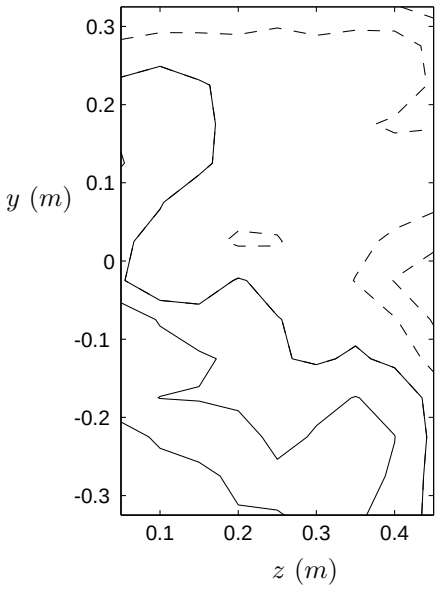

FIGURE 16. The temperature variation in a cross section area of the test section located 0.25 m from the entrance of the test section. The increment of each line is 0.025° C. Dashed lines represents negative values and solid lines positive values.

temperature in the upper and right parts of the cross section. This can be explained by the fact that the water enters the heat exchanger in the upper right corner of the cross section and exits at the lower right corner with a temperature difference between entering and exiting water of a few tenths of a degree leading to a colder right part of the cross section area. The small variation of temperature in the cross section indicates that the positioning of the heat exchanger is adequate and the flow rate through the heat exchanger is large enough, see section 2.4.2. The MTL wind-tunnel had originally, as a comparison, a temperature variation across the test section area of ± 0.2 °C, (Johansson (1992)), although significantly better results are now achieved (± 0.05 °C) with an improved temperature control system (Lindgren & Johansson (2002)).

Some types of measurements in the wind-tunnel can take many hours and it is normally important to maintain a constant temperature. It is important not only that the temperature is stable during long times, but also that the short time variation is small. The control loop used in the new wind-tunnel for all measurements was of PI type. The D, (derivative part), in the PID-regulator was not used, although it shortens the transient time when *e.g.* the wind-tunnel speed is changed, because it leads to a larger short time variation.

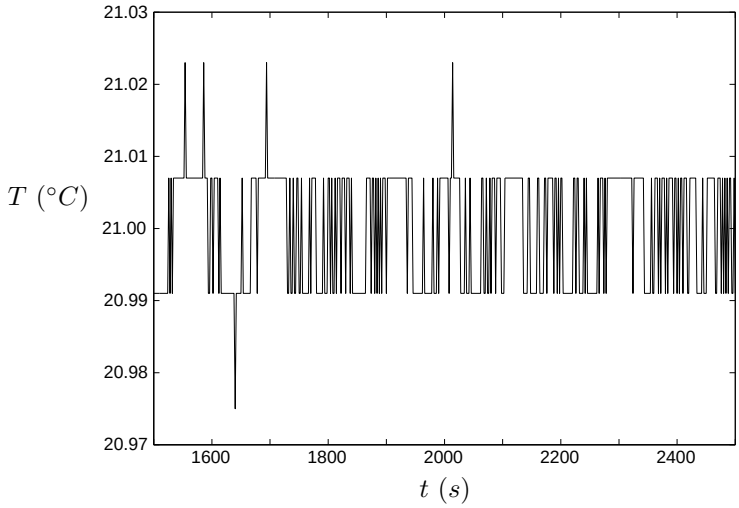

FIGURE 17. The temperature variation in time in the center of the test section 0.25 m from the its entrance.

The temperature was monitored for more than 4 hours and a window of 1500 s is shown in figure 17. The rest of the measurement shows a similar behavior. The 16 bit AD converter gives a resolution of 0.016°C and as seen in figure 17 the variation is less than ±0.03°C or 3 bits.

4.3. *Turbulence intensity measurement*

One of the most important aspects of the flow quality in a wind-tunnel is the level of turbulence intensity. During the design of the wind-tunnel, a lot of work was devoted to ensure that the parts used for turbulence damping, such as screens, honeycomb and contraction would work well, see section 2.5. The measurement of the turbulence intensity in both the streamwise and cross-stream directions were made to verify the quality of the design of these parts.

The turbulence intensity is defined as

$$I_{\mathrm{x}} = \frac{u_{\mathrm{rms}}}{U}, \tag{24}$$

$$I_{\mathrm{y}} = \frac{v_{\mathrm{rms}}}{U}, \tag{25}$$

$$I_{\mathrm{z}} = \frac{w_{\mathrm{rms}}}{U}, \tag{26}$$

where I_x, I_y and I_z are the turbulence intensities in the streamwise, the cross-stream vertical and the cross-stream horizontal directions, respectively, and U is the streamwise mean velocity.

One important aspect is to define what turbulence is in this case. There will always be flow variations with wave lengths of several meters containing a substantial part of the total turbulent kinetic energy. In this case we decided to include only flow structures with smaller wave length than 1.25 m. These measurements were made at a test section speed of about 25 m/s and the cut-off frequency, f_c, is 20 Hz using,

$$f_c = \frac{U}{\lambda_c} \tag{27}$$

where λ_c is the cut-off wave length. The choice of cut-off frequency is of course somewhat subjective. Here we chose the limiting wave length to be twice the mean of the vertical and horizontal side lengths.

The rms values can be calculated by summing up the square of the absolute value of the Fourier coefficients of the time signal. The high-pass filtering then consists of summing only over the frequencies above the cut-off frequency. The expressions for the three velocity components reads

$$u_{\mathrm{rms}} = \left(2 \sum_{k=N_c}^{N/2} |X_i|^2 \right)^{\frac{1}{2}}, \tag{28}$$

$$v_{\mathrm{rms}} = \left(2 \sum_{k=N_c}^{N/2} |Y_i|^2 \right)^{\frac{1}{2}}, \tag{29}$$

$$w_{\mathrm{rms}} = \left(2 \sum_{k=N_c}^{N/2} |Z_i|^2 \right)^{\frac{1}{2}}, \tag{30}$$

where X, Y and Z are the Fourier coefficients corresponding to the velocity time signals $u(x,y;t) - U(x,y)$, $v(x,y;t) - V(x,y)$ and $w(x,y;t) - W(x,y)$ respectively (with U, V, W denoting the time averaged values). N is the total number of samples and N_c is the summation index, k, corresponding to the frequency f_c.

To illustrate the distribution of kinetic energy over the frequencies the energy density function is calculated according to the following expression

$$\Phi(f_k) = 2N\Delta t |X_i(f_k)|^2 \quad k = 0, 1, \ldots, \frac{N}{2} \tag{31}$$

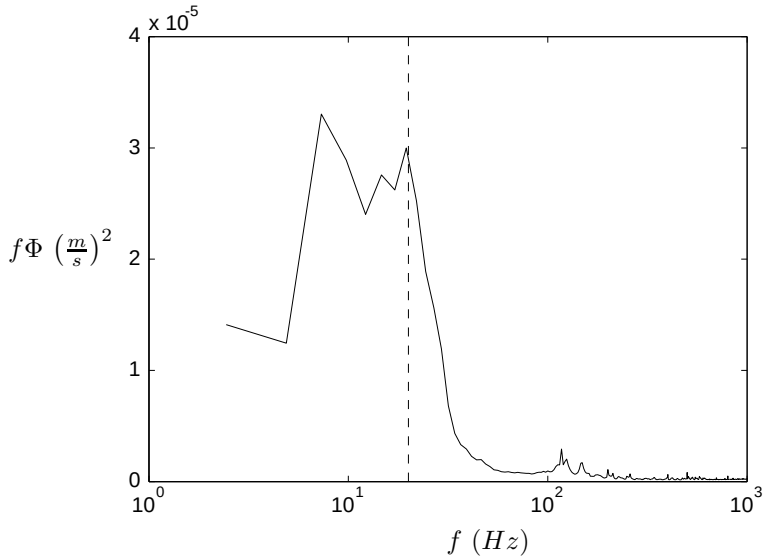

FIGURE 18. A typical power spectrum for the u velocity component in the core region of the test section. the dashed vertical line illustrates the cut-off frequency for the high-pass filter.

where $f_k = k/(N\Delta t)$. In figure 18 an example of a power spectrum for the streamwise velocity in the core region of the test section is shown. Note that most of the energy is located at very low frequencies. For the streamwise component the filtering removes about 50% of the energy as can be seen in figure 18 where the area under the curve to the left of the cut-off frequency is about similar in size to the area to the right. For the cross-stream components the effect of filtering is much smaller since less energy is located at low frequencies here. The cross-stream components are not affected by the waves traveling around the wind-tunnel circuit. This illustrates the purpose of the filtering which is to remove the influence of the traveling waves on the results. For comparison results for both filtered and unfiltered data are given in this paper. A comparison between the maximum values of the turbulence intensity for unfiltered and filtered data is shown in table 5.

The streamwise turbulence intensity over the measurement area for both unfiltered and filtered data is shown in figure 19. In the case of filtering the turbulence intensity is less than 0.04%, (see also table 5). In the center of the measurement area the turbulence intensity is less than 0.02%. This is very low especially considering the novel feature of expanding corners and the small cross section area of the test section. Most future experiments will be performed in this region of the test section cross section area. It is also comparable

TABLE 5. A comparison between filtered and unfiltered turbulence intensities in the core region of the test section.

Turb. Int.	filtered (20 Hz)	non-filtered
I_x	< 0.04 %	< 0.08 %
I_y	< 0.06 %	< 0.08 %
I_z	< 0.04 %	< 0.05 %

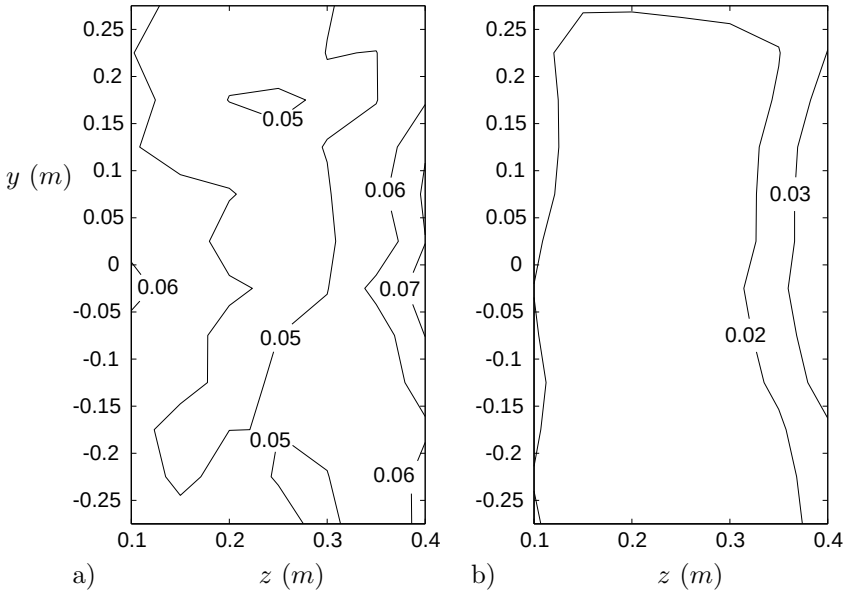

FIGURE 19. The streamwise turbulence intensity in a cross section area of the test section located 0.25 m from its entrance. a) non-filtered data, b) high-pass filtered data with cut-off frequency 20 Hz.

to the turbulence intensity measured in the MTL wind-tunnel under similar conditions, see Johansson (1992) and Lindgren & Johansson (2002).

For the unfiltered data the corresponding maximum intensity reaches 0.08% towards the right vertical wall but there is also an increase towards the left wall. (The flow is in the positive x-direction). In general the influence from the side walls is larger than the influence from the top and bottom walls. This can partly be explained by the shorter distance between the vertical walls compared to the horizontal walls. The more irregular pattern of the contours in the figure showing unfiltered data can be explained by the fact that the measurement time of each point is slightly too small to give good statistics for the low frequencies.

For the filtered vertical cross-stream component the turbulence intensity is 50% higher than for the streamwise component, *i.e.* less than 0.06% which is still very low compared to most wind-tunnels. The most noticeable feature of figure 20b is the strong gradient at the right wall. (The flow is in the positive x-direction). The gradient was also larger at this wall for the streamwise component but not as pronounced as here. The high turbulence level was first thought to be the result of a separation bubble at this wall located in the contraction. An investigation was performed using tufts to detect the separation. The result of the investigation was however that no separation bubble could be detected. Other possible reasons could be *e.g.* rough joints between wind-tunnel parts or vertical vibrations of the probe at these positions. As will be seen below the contribution from low frequency structures to the high turbulence intensity is substantial in this region.

The contours of the unfiltered vertical cross-stream intensity in figure 20a have a similar pattern to those in figure 20b. The effect of the filtering is not as pronounced for this component as for the streamwise one. There is, however, a larger filtering effect close to the right vertical wall indicating that the contribution to the high turbulence level encountered here is mainly from low frequency components. The maximum value of the unfiltered intensity is less than 0.8% which is comparable to the streamwise case, see table 5. In the central region of the measurement area the level of turbulence intensity is less than 0.03% which is very low, although this region is fairly small.

The horizontal component of the cross-stream turbulence intensity is in the filtered case less than 0.04%. The turbulence intensity is fairly evenly spread out over the measurement area with only a slight increase towards the edges and a very small central region where the intensity is less than 0.02%. For most of the measurement area the level is below 0.03%, see figure 21b. There is no large gradient at the right vertical wall as was the case for the vertical cross-stream component indicating that probe vibrations could be the cause for the strong gradient since it effects the streamwise and vertical components but not the horizontal component. (The flow direction is as before into the paper).

The unfiltered intensity for the horizontal component is also evenly distributed over the measurement area with slightly lower values in the central region and higher towards the wall as is expected. The value of the turbulence intensity is less than 0.05% over the entire region and less than 0.03% in a fairly large core region.

The filtered values of the cross-stream components is comparable to the values found in the MTL wind-tunnel, excluding the high values of vertical component at the right wall. This is somewhat surprising since the size of this wind-tunnel is substantially smaller, which makes it more difficult to achieve low values, because the walls influence a relatively speaking larger part of the cross section area. One could also expect some separation on the guide vanes

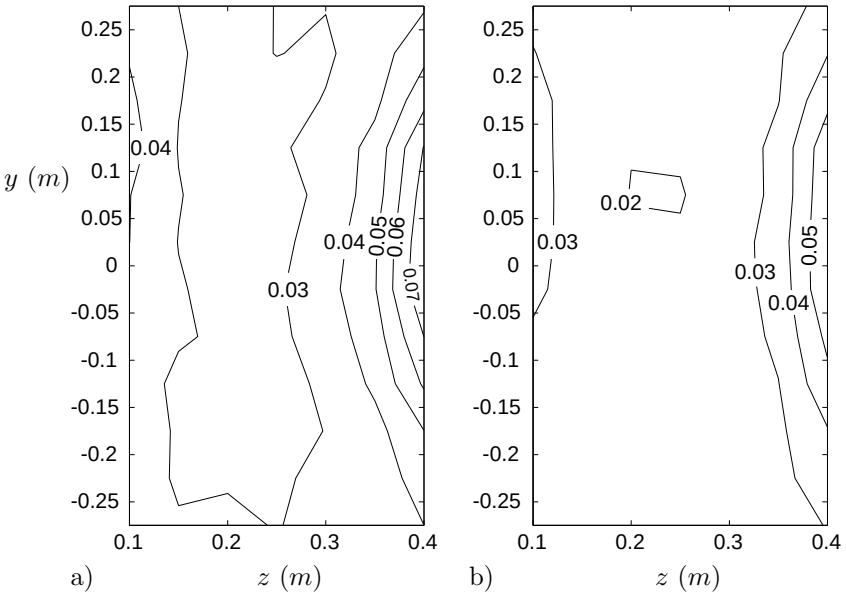

FIGURE 20. The vertical crosswise turbulence intensity in a cross section area of the test section located 0.25 m from its entrance. a) non-filtered data, b) high-pass filtered data with cut-off frequency 20 Hz.

in the fourth corner due to the very low chord Reynolds numbers found there, which could have a negative influence on the turbulence levels. However one should keep in mind that the data presented for the MTL wind-tunnel spans tunnel velocities between 10 and 60 m/s while this tunnel was only tested at 25 m/s which is the design tunnel velocity for which the wind-tunnel is optimized.

4.4. *Noise measurement*

The lack of insulation material in the wind-tunnel circuit except in the two silencers surrounding the fan made it particularly important to check the noise level in the wind-tunnel lab. As a comparison it can be noted that the MTL wind-tunnel has insulated walls throughout most of the wind-tunnel circuit. As seen in figure 22, the noise level outside the test section is very low. Actually it is impossible to hear the wind-tunnel running at a speed of 25 m/s if it is not totally quiet elsewhere in the room. The noise level outside the fan is slightly higher but the machinery is located on a lower level and the sound is effectively blocked by the floor. The reason for the somewhat irregular behavior of the curves in figure 22, especially that representing the position outside the fan, is that the load on the fan bearings varies with rpm leading to a mechanically induced noise increment at some fan speeds.

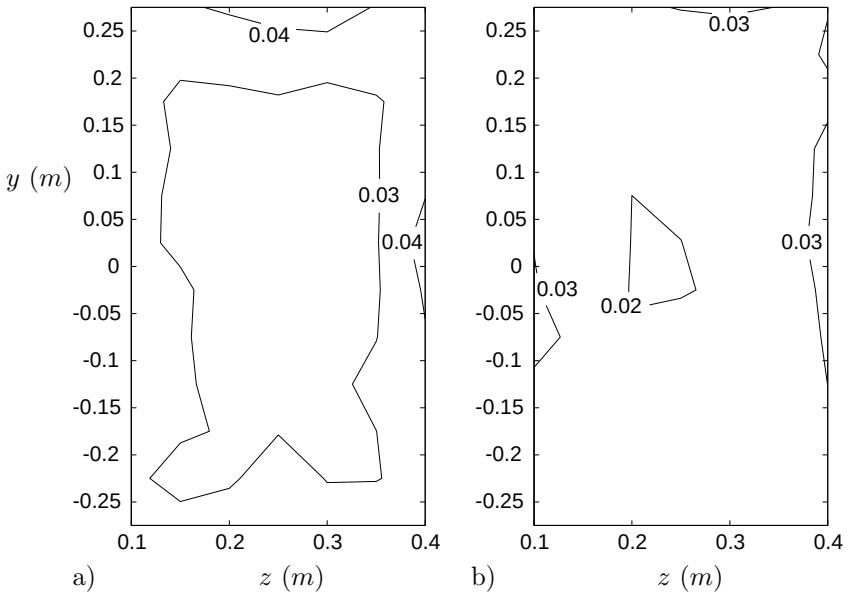

FIGURE 21. The horizontal crosswise turbulence intensity in a cross section area of the test section located 0.25 m from its entrance. a) non-filtered data, b) high-pass filtered data with cut-off frequency 20 Hz.

4.5. *Guide-vane performance*

A central design aspect for this wind-tunnel is the use of expanding corners, see section 2.3. To get a good comparison with the experiments and calculations presented in Lindgren *et al.* (1998), the chord Reynolds number was chosen to be around 200000. The most critical corner in terms of pressure-loss and flow quality is corner 1, located closely behind the test section, see figure 2. This is due to the disturbances often generated in the test section from measurement equipment, such as traversing arms, boundary layer plates or cylinders. The measurement consisted in traversing a pitot tube across the guide-vanes at the center of their span and also to measure the static pressures upstream and downstream of corner 1. This way of setting up the experiment should give close to two-dimensional results. The measurements in Lindgren *et al.* (1998) were performed in a similar way. The calculations in Lindgren *et al.* (1998) were purely two-dimensional on an infinite cascade with undisturbed incoming flow. Therefore the wall side boundary layers were excluded when calculating the total pressure-loss coefficient in the new experiment. The total pressure-loss coefficient is defined as

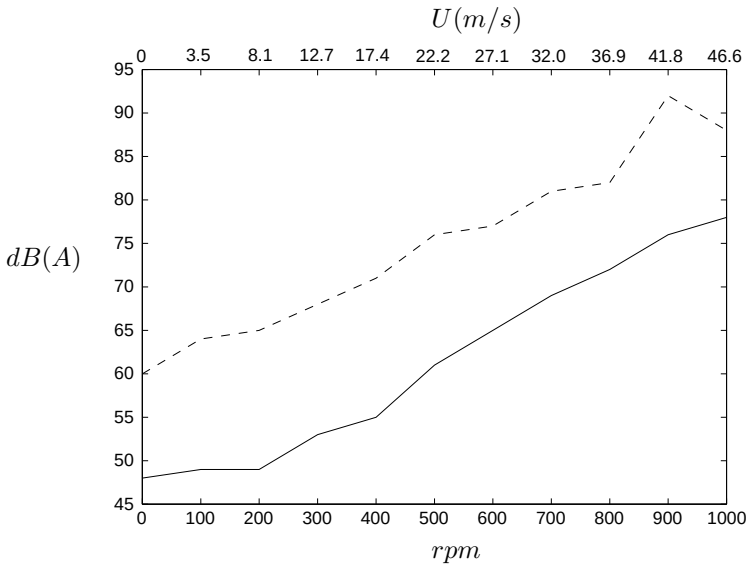

FIGURE 22. The Noise level outside the test section, —, and outside the fan, ––. Fan rmp scale (bottom) Test section velocity scale (top)

$$\frac{\Delta H}{q_0} = \frac{p_{t0} - \overline{p_{t1}}}{q_0} \tag{32}$$

where p_{t0} is the total pressure upstream the corner and $\overline{p_{t1}}$ is the mean total pressure downstream the corner. Expressed in the three measured pressure differences, ($p_{t0} - p_1$, $p_{t1}(y) - p_1$ and $p_{t0} - p_0$), the equation reads

$$\frac{\Delta H}{q_0} = \frac{p_{t0} - p_1 - \frac{1}{nh_1}\int_0^{nh_1} (p_{t1}(y) - p_1)\, dy}{p_{t0} - p_0} \tag{33}$$

where p_0 and p_1 are the static pressure upstream and downstream the corner, n is the number of vanes over which the integration is performed and h_1 is the outlet distance between the vanes, see figure 5. The results show good agreement between calculations and experiments with a total pressure-loss coefficient for the calculations in Lindgren *et al.* (1998) of 0.041 and this experiment with a total pressure-loss coefficient of 0.047. Remember that the calculations are performed on a non-disturbed purely two-dimensional flow completely free of the three-dimensional effects which influences the measurements and leads to higher pressure-loss. The value of the total pressure-loss coefficient of 0.047 is very good even when compared to most non-expanding guide-vane corners which often have values of the total pressure-loss coefficient above 0.1.

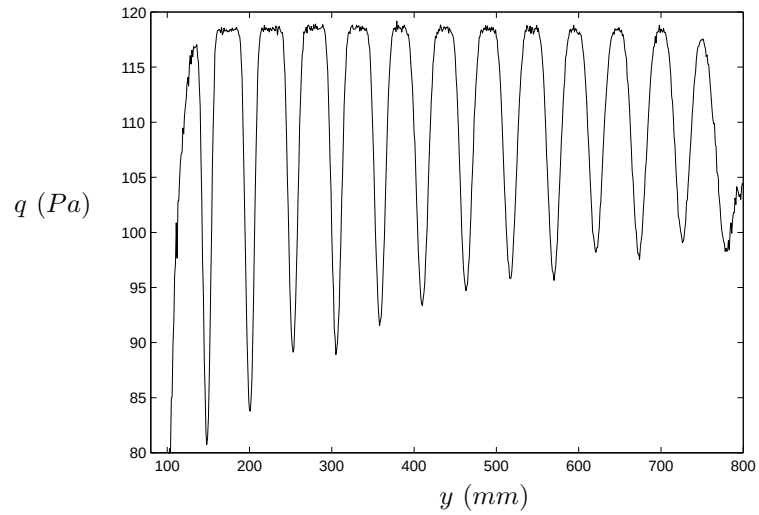

FIGURE 23. The variation of the dynamic pressure across the guide-vanes at their spanwise center position, $Re_c = 205000$.

In figure 23 the wakes behind the guide-vanes can be seen with the trailing edges of the vanes located at a y position coinciding with the minimum values of dynamic pressure, q. To the right in figure 23 the wakes are wider but not so deep. This is because the distance between the traversed pitot tube and the guide-vanes is larger there, see figure 14.

Note also the thickness of the boundary layers. It can be seen in the left part of the figure 14 that the boundary layer here is about 15 cm thick. The guide-vanes, however, still seem to cope well with these adverse conditions.

5. Concluding remarks

The design of the new wind-tunnel is a success. All considered flow quality factors, such as mean flow variations, turbulence intensities, temperature variations and noise are well within the expected levels. It is proven that it is possible to include expanding corners into the wind-tunnel design without deteriorating the flow quality or increasing the wind-tunnel circuit total pressure-loss. The use of a standard industrial fan/motor solution with an AC motor and frequency converter has not had a negative effect on the flow quality but some disturbances on the electrical mains affecting *e.g.* temperature and hot-wire anemometry measurements have been detected. It was also possible to eliminate these disturbances by improved cabling. The maximum speed is 48 m/s with an empty test section, but it can be increased further by over-riding the maximum rpm allowed for the fan, without over-heating the motor. This

can be done for shorter periods of time, (up to a few hours), without risk of damaging the fan bearings.

The total pressure-loss of the wind-tunnel circuit represents a moderately high power factor value of 0.46, see section 4.1, but it is important here to consider the size and length of the wind-tunnel test section and the flow quality improving devices implemented leading to a higher total pressure-loss.

The variation of total pressure in the test section at a test section velocity of 25 m/s is below $\pm 0.1\%$. This is equivalent to a velocity variation of less than $\pm 0.05\%$. No clear trend in the variation over the test section cross section can be seen. The small variations present are irregularly distributed and the amplitude is of the same order of magnitude as the accuracy of the measurements.

The temperature variation in the test section at a test section speed of 25 m/s is very small. Over the cross section in the test section the variation is less than ± 0.07°C and the variation over a time period of 4 hours is less than ± 0.03°C in the center of the cross section. A clear trend of the temperature variation over the cross section can be seen.

The turbulence levels at a test section speed of 25 m/s are very low, see section 4.3. All components of the turbulence intensity are below 0.04% in the core region of the test section cross section area. These values are calculated with a high-pass filter at 20 Hz eliminating flow structures larger than 1.25 m. Without filtering, the values of the turbulence intensities are slightly higher with a streamwise turbulence intensity of less than 0.06% and for the cross flow directions it is less than 0.08%. These levels are still very low proving that the honeycomb, screen package and contraction are complying fully to our expectations.

The noise level outside the fan and outside the test section pressure equalizing slit is satisfactorily low, see section 4.4. Outside the test section the noise level is about 63 dB(A) at a speed of 25 m/s and about 74 db(A) at maximum speed. This low noise level is achieved by a low rpm fan of relatively large size. The larger diameter of the fan is made possible by the use of expanding corners that leads to a fast increase in the wind-tunnel cross section area.

In the experiments and calculations of Lindgren *et al.* (1998) it was found that expanding corners represent a good design concept for obtaining a compact tunnel circuit with low pressure losses. The measurements on the expanding corners in the new wind-tunnel shows that this is indeed the case with a quasi two-dimensional total pressure-loss coefficient of 0.047 at a chord Reynolds number of about 200000. The earlier experiments with a slightly different guide-vane had a total pressure-loss coefficient of 0.057 at the same Reynolds number and the two-dimensional calculations on an infinite cascade pointed to a total pressure-loss coefficient of 0.041 at the same Reynolds number, see Lindgren *et al.* (1998). The slightly higher value for the experiment than the

calculation with the new guide-vane is expected because the flow condition in reality is never as good as the disturbance free, purely two-dimensional flow condition in the calculation. However, the new experimental result is clearly better than the earlier result with the other guide-vane proving that the optimization of a new guide-vane for expanding corners was successful. The good flow quality in the test section also indicates that the new guide-vane is able to perform also at the very low chord Reynolds number encountered in corner 4. These results prove that the use of expanding corners can be implemented in wind-tunnel constructions saving space and money without sacrificing flow quality or increasing the total pressure-loss of the wind-tunnel circuit noticeably.

6. Acknowledgment

The authors would like to thank Jens Österlund for his support and suggestions during the work and Ulf Landén and Marcus Gällstedt for their help in assembling of the wind-tunnel parts and manufacture measurement equipment. Finally we wish to thank The Göran Gustafsson Foundation and The Swedish Research Council for financial support.

References

Angele, K. 2000 PIV measurements in a separating turbulent APG boundary layer. TRITA-MEK 2000:15. Lic. Thesis, Department of Mechanics, KTH.

Baines, W. D. & Petersen, E. G. 1951 An investigation of flow through screens. *Trans. ASME* **73**, 467–480.

Batchelor, G. K. 1976 *The theory of homogeneous turbulence*. Camebridge University Press.

Borger, G. G. 1976 The optimization of wind tunnel contractions for the subsonic range. *Tech. Rep.* TTF 16899. NASA.

Bradshaw, P. & Pankhurst, R. C. 1964 The design of low-speed wind tunnels. *Progress in aeronautical sciences* **6**, 1–69.

Çabuk, H. & Modi, V. 1992 Optimum plane diffusers in laminar flow. *J. Fluid Mech.* **237**, 373–393.

Collar, A. R. 1936 Some experiments with cascades of aerofoils. A.R.C. Technical Report 1768. Aeronautical research committee.

Downie, J. H., Jordinson, R. & Barnes, F. H. 1984 On the design of three-dimensional wind tunnel contractions. *J. Royal Aeronautical Society* pp. 287–295.

Drela, M. & Giles, M. B. 1987 Viscous-inviscid analysis of transonic and low Reynolds number airfoils. *AIAA* **25** (10), 1347.

Drela, M. & Youngren, H. 1995 *A users guide to MISES 2.1*. MIT Computational Aerospace Sciences laboratory.

Fox, R. W. & Kline, S. J. 1962 Flow regime data and design methods for curved subsonic diffusers. *Trans. ASME, J. Basic Engineering, Ser. D* **84**, 303–312.

Friedman, D. & Westphal, W. R. 1952 Experimental investigation of a 90° cascade diffusing bend with an area ratio of 1.45:1 and with several inlet boundary layers. TN 2668. NACA.

Ganesan, V., Suzuki, K., Narayana, P. A. & Chithambaran, V. K. 1991 Investigations of mean and turbulent flow characteristics of a two dimensional plane diffuser. *Experiments in Fluids* **10**, 205–212.

Giles, M. B. & Drela, M. 1987 Two-dimensional transonic aerodynamic design method. *AIAA Journal* **25** (9), 1199.

Görtler, H. 1941 Instabilität laminarer Grenzschichten an konkaven Wänden gegenüber dreidimensionalen Störungen. *ZAMM* **21**, 250–252.

Groth, J. 1991 On the modelling of homogeneous turbulence. *Tech. Rep.*. Dep. of Mechanics, KTH, SE-100 44 Stckholm.

Groth, J. & Johansson, A. V. 1988 Turbulence reduction by screens. *J. Fluid Mech* **197**, 139–155.

Johansson, A. V. 1992 A low speed wind-tunnel with extreme flow quality-design and tests. *Proc. the 18:th ICAS Congress* pp. 1603–1611.

Johansson, A. V. & Alfredsson, P. H. 1988 *Experimentella metoder i strömningsmekaniken*. Department of Mechanics, Royal Institute of Technology.

Kröber, G. 1932 Schaufelgitter zur Umlenkung von Flussigkeits-Strömung. *Ingenieur-Archiv* **3**, 516.

Laws, E. & Livesey, J. 1978 Flow through screens. *Ann rev Fluid Mech.* **10**, 247–266.

Lindgren, B. 1999 Development of guide-vanes for expanding corners with application in wind-tunnel design. TRITA-MEK 1999:8. Department of Mechanics, KTH.

Lindgren, B. & Johansson, A. V. 2002 Evaluation of the flow quality in the low-speed MTL wind-tunnel. TRITA-MEK 2002:13. Department of Mechanics, KTH.

Lindgren, B., Österlund, J. M. & Johansson, A. V. 1998 Measurement and calibration of guide-vane performance in expanding bends for wind-tunnels. *Experiments in Fluids* **24**, 265–272.

Loehrke, R. I. & Nagib, H. M. 1976 Control of free-stream turbulence by means of honeycombs: A balence between suppression and generation. *J. Fluids Engineering* pp. 342–353.

Malmer, I. 1933 Tekniska högskolans flygtekniska laboratorium. *Teknisk Tidskrift* .

Mehta, R. D. & Hoffmann, P. H. 1987 Boundary layer two-dimensionality in wind tunnels. *Experiments in Fluids* **5**, 358–360.

Michel, U. & Froebel, E. 1988 Lower limit for the velocity fluctuation level in wind tunnels. *Experiments in Fluids* **6**, 49–54.

Mikhail, M. N. & Rainbird, W. J. 1978 Optimum design of wind tunnel contractions, paper 78-819. In *AIAA 10th Aerodynamic Testing Conference*.

Nash, E. C., Lowson, M. V. & McAlpine, A. 1999 Boundary-layer instability noise on airfoils. *J. Fluid Mech.* **382**, 27–61.

Österlund, J. M. & Johansson, A. V. 1999 Turbulent boundary layer experiments in the MTL wind-tunnel. TRITA-MEK 1999:16. Department of Mechanics, KTH.

Prandtl, L. 1932 Herstellung einwandfreier Lufstöme (Windkanäle). Handbuch der Experimentalphysik, Leipzig, Germany, vol 4, part 2,p.73. *Naca Tech. Mem.* **726**.

Rae, W. H. & Pope, A. 1984 *Low-speed wind tunnel testing.*, 2nd edn. John Wiley & sons.

Reneau, L. R., Johnson, J. P. & Kline, S. J. 1976 Performance and design of straight, two-dimensional diffusers. *Trans. ASME, J. Basic Engineering* **89**, 141–156.

Sahlin, A. & Johansson, A. V. 1991 Design of guide vanes for minimizing the pressure loss in sharp bends. *Phys. Fluids A* **3**, 1934–1940.

Scheiman, J. & Brooks, J. D. 1981 Comparison of experimental and theoretical turbulence reduction from screens, honeycomb and honeycomb-screen combinations. *JAS* **18**, 638–643.

Seidel, M. 1982 Construction 1976-1980. design, manufacturing, calibration of the German-Dutch wind tunnel (DNW). *Tech. Rep.*. Duits-Nederlandese Windtunnel (DNW).

Shaw, R. 1960 The influence of hole dimensions on static pressure measurements. *J. Fluid Mech.* **7**, 550.

Sjögren, T. & Johansson, A. V. 1998 Measurement and modelling of homogeneous axisymmetric turbulence. *J. Fluid Mech* **374**, 59–90.

Taylor, G. & Batchelor, G. K. 1949 The effect of wire gauze on small disturbances in a uniform stream. *Quart. J. Mech. and App. Math.* **2**, part 1,1.

Waitman, B. A., Reneau, L. R. & Kline, S. J. 1961 Effect of inlet conditions on performance of two-dimensional subsonic diffusers. *Trans. ASME, J. Basic Engineering* **83**, 349–360.

Wolf, H. 1957 Messungen im Nachlauf eines Gleichdruckgitters für 90-umlenkung. *Maschinenbautechnik* **6** (10), 539.

Wolf, S. 1969 Effects of nonuniform inlet velocity profiles on flow regimes and performance in two-dimensional diffusers. *Trans. ASME, J. Basic Engineering* **91**, 462–474.

Youngren, H. & Drela, M. 1991 Viscous/inviscid method for preliminary design of transonic cascades. In *AIAA, SAE, ASME, and ASEE, Joint Propulsion,Conference, 27th.*.